INTERNATIONAL JOURNAL OF AUTOMOTIVE AND MECHANICAL ENGINEERING
ISSN: 2229-8649 e-ISSN: 2180-1606
VOLUME 23, ISSUE 1, 2026, 13190 - 13199
DOI: https://doi.org/10.15282/ijame.23.1.2026.3.1001

RESEARCH ARTICLE

Quality of friction stir welding joints on aluminum 1100 thin plates

Febri Budi Darsono[1]*, Akhmad Nurdin[2], Fajar Paundra[3], Alvreando Kaleb Thomas[4], Tasih Mulyono[5], Muhammad Irfan Nuryanta[1], Hendrix Noviyanto Firmansyah[1], Aldias Bahatmaka[1], Deni Fajar Fitriyana[1], Kriswanto[1], Rahmat Doni Widodo[1], and Nurul Muhayat[6]*

[1]Department of Mechanical Engineering, Universitas Negeri Semarang Sekaran, Gunung Pati, Semarang, 50299, Indonesia
[2]Department of Manufacturing Design Engineering, Universitas Tidar, Magelang Utara, Jawa Tengah, 56116, Indonesia
[3]Department of Mechanical Engineering, Faculty of Industrial Technology, Institut Teknologi Sumatera, Lampung, 35365, Indonesia
[4]Department of Quality Control, PT Ramai Jaya Abadi Murung Pudak, Tabalong, Kalimantan Selatan, 71571, Indonesia
[5]Politeknik Teknologi Nuklir Indonesia Caturtunggal, Depok, Sleman Yogyakarta, 55281, Indonesia
[6]Department of Mechanical Engineering, Universitas Sebelas Maret, Surakarta, 57126, Indonesia

Abstract – The Aluminum 1100 series is widely used because of its high corrosion resistance and ductility. Joining aluminum with conventional welding presents challenges due to its poor weldability. Friction Stir Welding (FSW) is a solid-state joining process in which heat is generated by the tool's rotation, with the pin and shoulder rubbing against the material to be welded, stirring it. The FSW process can reduce welding issues when joining aluminum materials. The quality of the joint formed by friction stir welding depends on the welding parameters, as evidenced by numerous prior investigations. However, previous research has been limited to the mechanical strength of welded joints, using destructive testing methods. This allows researchers to examine the quality of welded joints using nondestructive testing. Researchers focus on the quality of friction-stir-welded joints on an AA 1100 thin plate. The tool used has three flat sides, with a tool pin and shoulder diameter ratio of 1:3. The parameters used were variations in the tool's lateral tilt angle, with values of 00, 0.50, and 10. The travel speed was 45 mm/minute with a tool rotation of 1860 rpm. The clamp/fixture was made of S45C, a heat-treated material; the backing plate was mild steel. The AA 1100 material, thicker than 2 mm, undergoes welding. The quality of FSW joints was inspected using nondestructive testing methods, including visual, radiographic, and eddy-current testing. In contrast, mechanical strength was assessed by tensile testing to validate the nondestructive test. The results indicated that tilt angle 00 had no defects, tilt angle 0.50 had tunneling or voids, and tilt angle 10 had defects in the form of material gaps. When the tilt angle was changed to 00, the tensile strength was 85.53 MPa, and the joint efficiency was 78%. When the tilt angle was set to 0.50 and 10, the tensile strength dropped to 61.84 MPa and 71.91 MPa, respectively.

Article History
Received : 28 April 2025
Revised : 25 August 2025
Accepted : 23 December 2025
Published : 02 March 2026

Keywords
Friction stir welding
Weld quality
Aluminum 1100
Nondestructive test
Tensile strength

1. Introduction

The Aluminum 1100 series is widely used for its good corrosion resistance and high toughness; it is used in the nuclear sector [1], defense [2], the manufacture of radiator components and fuel tanks [3], and sheet metal work [4]. Combining aluminum with conventional welding can be challenging because it is difficult to weld. The process can cause cracks, holes, weakening, shrinkage, and the formation of an oxide layer [5-9]. Friction Stir Welding (FSW) is a welding technique patented by TWI in 1991. It is a solid-state joining process, with heat generated by the tool's rotation pin and shoulder that rubs and stirs the material to be welded [10]. The tool is made of non-consumable material and is more difficult to weld than the base material; the heat generated by the rubbing tool affects the material's stirring throughout the welding process [11-13]. The tools used in FSW account for 75% of the weld joint. These tools change the microstructure, grain uniformity, and material flow [14-15]. Muhayat et al. [16] conducted FSW research on AA5052-H32 and found that the shape of the pin profile contributes to the weld joint. Modifications in cylindrical pin profiles, comprising two flat-sided and three flat-sided preheat variations (150–300 ^{0}C), revealed flaws in the macrographs of the two flat-sided tools. Their mechanical properties improved at a preheat temperature of 250 ^{0}C. At the same time, the three flat-sided tools had better mechanical properties than the two flat-sided tools, with a 12.2% increase in joint efficiency. In addition, the shoulder diameter and the pin tool ratio affect the mechanical strength; a shoulder diameter to pin tool ratio of 3:1 shows significant mechanical strength [17], which was also done through trial and error by Mehta et al. [18], this indicates that the three flat-sided pin tool profiles have the best welding results compared to the cylindrical and two flat-sided pin tool profiles. In contrast, the shoulder diameter ratio with the pin tool of 3:1 shows significant results on mechanical strength. Hence, this is a consideration for researchers to use these tool dimensions.

FSW parameters affect the welding joint; Kumar et al. [19]. According to FSW research on AA1100, the parameters are the rotation tool and the travel speed. The rotation speeds used were 1800, 2100, and 2400 rpm, and the travel speeds were 40, 45, and 50 mm/min. Welding joints created with threaded cylindrical pin tools exhibit superior qualities compared to those formed with straight cylindrical pin tools, particularly for tensile strength and elongation. At 1800 rpm and 50 mm/min, the joint efficiency was 90%, and at 2400 rpm and 45 mm/min, it had the most elongation of 8.38%. This indicates that it has greater flexibility than straight cylindrical pin tools. This shows that the optimum parameters are obtained in the rpm range of 1800 rpm and 2400 rpm with welding speeds of 45 mm/min and 50 mm/min, so the researchers consider tool rotation between 1800 and 2400 rpm, while the welding speed uses 45 mm/min. Utilizing the appropriate fixture during FSW welding on thin aluminum plates is crucial to ensure the metal can withstand deformation

***CORRESPONDING AUTHOR | Febri Budi Darsono** | ✉ febribudi@mail.unnes.ac.id

and stress induced by the FSW tool's heat. Ahmed et al. [20] conducted a study on FSW of a thin AA6061-T6 plate (0.5 mm) using a stainless steel fixture, a backing plate, and asbestos on the cover plate to retain heat, leading the researchers to consider using clamps/fixtures and backing plates during FSW. Tsarkov et al. [21] investigated the effect of the tilt angle on the tensile strength of friction-stir-welded joints. The tensile strength varied from 0° to 3° while maintaining a constant tool configuration and a constant ratio of travel speed to rotational speed. The temperatures of the tool and the forging material during welding on the advancing side (AS) peaked at 312°C to 442°C at the weld center. The tilt angle influences the heat generated and the material flow in FSW joints; Dialami et al. conducted this work [22] with tool angles of 0^0 and 2.5^0. Elevated temperatures render the material more pliable, increasing friction in the tool region and intensifying it with the introduction of a tilt angle, thereby mitigating the incidence of faults. Yogaraj et al. [23] conducted parameter optimization for FSW of aluminum 1100, including variations in the pin profile (tapered and threaded), travel speed, tilt angle, and tool rotation. The dominant parameter was travel speed, along with changes to tilt angle variations and travel speed using a cylindrical tool rotating at 800 rpm, 25 mm/min, 1^0; 35 mm/min, 1.5^0; 45 mm/min, 2^0, which showed a decrease in tensile strength of 99.45, 82.35, and 71.65 MPa. This also occurred during a tool rotation of 1000 rpm with cylindrical tools: 25 mm/min, 1^0; 35 mm/min, 1.5^0; and 45 mm/min, 2^0, which showed decreases in tensile strength of 84.65, 79.45, and 68.85 MPa, respectively. The elevated temperature in the tool and material, together with the increased tip angle, tool rotation, and travel speed, results in plastic deformation and the creation of an imperfection flash, thus reducing its strength, from this data, the researcher considered using a tilt angle tool that has not been disclosed, namely a range between 0^0 and 1^0, to see whether there is a decrease in tensile strength or an increase in tensile strength.

Testing evaluates the quality of a weld. Destructive testing includes metallography, hardness, and tensile-strength assessments, whereas nondestructive testing encompasses visual inspections, penetrant tests, and radiography. Radisavljevic et al.[24] examined the influence of R/v on the quality and mechanical attributes of FSW 2024-T351, where R denotes the tool rotation, and v represents the welding speed. The tool rotation speeds of 750, 950, and 1180 rpm, along with a welding speed of 73 to 190 mm/min, resulted in joint efficiencies of 52.2% to 82.3%, with optimal quality parameters of R/v at 8.06, 10.17, and 10.27. These characteristics enable the pin to convey material appropriately to fill the joint gap and avert tunneling. The quality of the weld can also be assessed by evaluating its strength. Wu et al. [25] conducted friction-stir welding studies on AA 7075 using tools made of H-13 and WC-Co materials. The tool's rotation and travel speed were adjusted from 400 to 800 rpm and 50 to 150 mm/minute, respectively. An examination of the FSW weld joint reveals that the influence of heat input from the preceding parameters can indicate weld quality. EBSD analyses of the weld nugget zone and base material regions can elucidate the grain size and boundary ratio. They obtained a hardness of 148 HV, a tensile strength of 492.3 MPa, and a maximum elongation of 6.2%. All three tests functioned effectively 87.4% of the time. Friction stir welding parameters significantly influence the quality of welded joints, as evidenced by numerous prior investigations. However, the welding quality data presented in these studies is limited to mechanical strength, determined by destructive tests. Researchers can conduct this research by using minimal data on welding quality obtained from nondestructive tests. Researchers concentrate on the "quality of friction stir welding joints on AA 1100 thin plate." The inspection of FSW joint quality uses nondestructive testing methods, including visual, radiographic, and eddy-current testing. At the same time, mechanical strength is evaluated through tensile testing, which serves to validate the nondestructive tests.

2. Materials and Methods

The material used was AA 1100, with a specimen size of 100×120×2 mm; the tool rotation direction was clockwise; the lateral tool tilt toward the RS variations were 0^0, 0.5^0, and 1^0; the FSW welding scheme can be seen in Figure 1; and the FSW welding parameters can be observed in Table 1.

Table 1. FSW Parameters

Rotation Speed (RPM)	1860
Welding Speed (mm/min)	45
Plunge depth (mm)	1.8
Lateral Tool Tilt Angle (^{0})	0, 0.5, and 1
Shape Tools	Three flat sides

The tool is made from SKD 61 material and undergoes a heat treatment process [15], achieving a hardness of 55 HRC. The tool profile has three flat sides, with a tool pin length of 1.8 mm and a shoulder diameter of 12 mm; the ratio of the tool pin diameter to the shoulder diameter is 1:3; the tool's shape is shown in Figure 2. The clamping and backing plate process is shown in Figure 3. Heat-treated S45C material is used for the clamp, while mild steel is used for the backing plate. Nondestructive testing (NDT) and destructive testing (DT) were conducted. The NDT was visual testing in accordance with PN-EN ISO 25239-5 [26]. Table 2 presents the imperfection criteria, with radiography testing performed on the Rigaku RF-200EG-S3 and eddy current testing conducted on the Mentor EM Portable machine. Figure 4 presents the FSW test coupon for tensile testing. The standard was ASTM E8 [27] with the tensile speed of 1 mm/minute. The DT testing used the Universal Testing Machine type UN-7001-LC30.

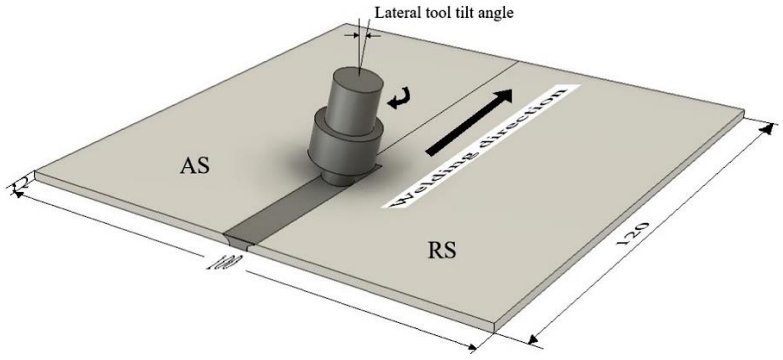

Figure 1. FSW welding schematic

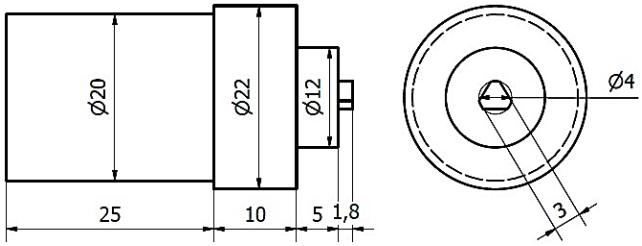

Figure 2. FSW tool shape

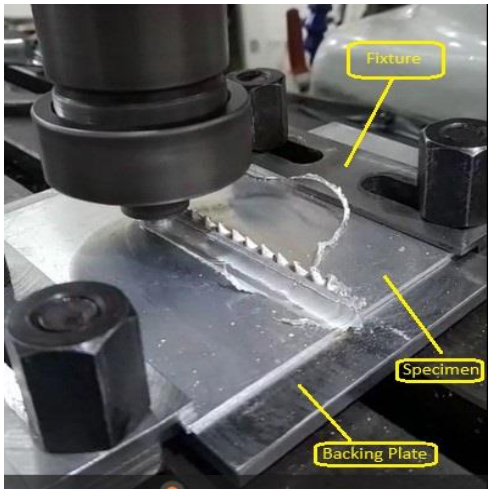

Figure 3. Specimen clamping and FSW process

Table 2. FSW joint imperfection, based on PN-EN ISO 25239-5 [26]

No	Imperfection	Acceptance
1	Incomplete penetration	Not permitted
2	Excess penetration	≤ 3 mm
3	Toe flash (flash)	Acceptable size of imperfection in accordance with the designer's requirements
4	Linear misalignment	h ≤ 0,2t max 2 mm
5	Underfill	h ≤ 0,1t max 0.5 mm
6	Irregular width	Acceptable size of imperfection in accordance with the designer's requirements
7	Irregular surface	Acceptable size of imperfection in accordance with the designer's requirements

t = nominal thickness base metal
h = height imperfection
d = length of an elongated cavity

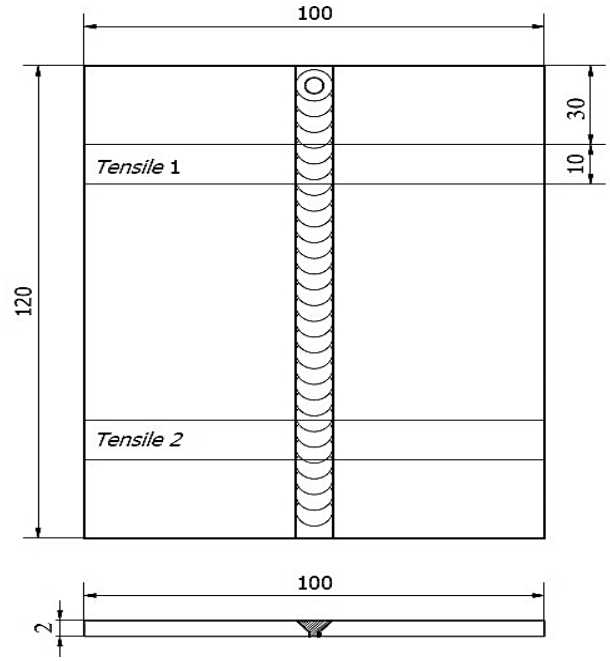

Figure 4. FSW coupon test

3. Results and Discussion

3.1 Visual Inspection Interpretation

Welding joints with friction on AA 1100 that were 2 mm thick and had tilt angles of 0^0, 0.5^0, and 1^0 are shown in Figure 5 as surface welds before finishing, and in Figures 6(a) and 6(b) as surface welds after finishing and bottom welds. Figure 5 shows that the lateral tilt angles of 0^0, 0.5^0, and 1^0 exhibited imperfections in the form of flash, indicated by the letter A. High rpm and welding speeds caused plasticized material to flow, resulting in flash imperfections at the weld edge. Furthermore, the welding speed alters the flow distribution during stirring, resulting in a more evenly mixed material but thinner. The effect of flash causes a reduction in material thickness [15, 28-29]. Table 3 illustrates the transition from three lateral tilt angle changes of 0°, 0.5°, and 1° to 0.2, 0.5, and 0.3 mm; however, the maximum value of 0.5 mm remained within the acceptance standards.

Figure 5. Surface weld unfinishing

Figures 6(a-b) show the results of FSW welding with lateral tilt angle variations of 0^0, 0.5^0, and 1^0. The images show no defects because they meet the acceptance criteria; details are shown in Table 3. The friction stir weld results after visual testing were accepted for the three tilt angles, so the following nondestructive test process was continued with radiography. Figure 7 displays the radiographic results for lateral tilt angles of 0^0, 0.5^0, and 1^0.

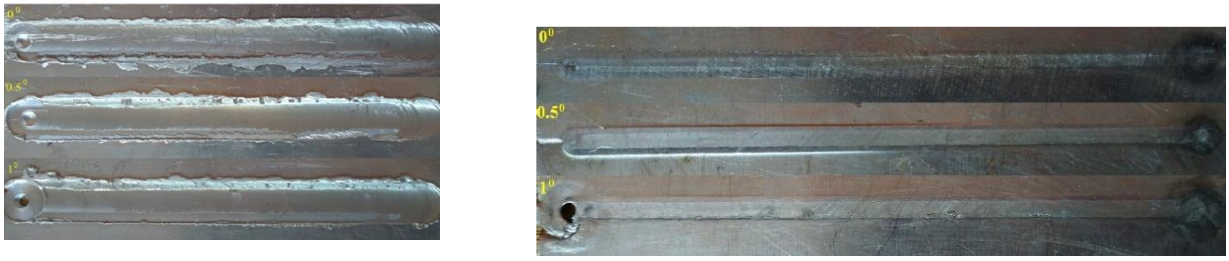

(a) (b)

Figure 6. (a) Surface weld, (b) bottom weld

Table 3. Visual interpretation based on PN-EN ISO 25239-5

No.	Imperfection	Acceptance	Results		
			0^0	0.5^0	1^0
1	Incomplete penetration	Not permitted	-	-	-
2	Excess penetration	≤ 3 mm	0 mm	0 mm	0 mm
3	Toe flash (flash)	Acceptable size of imperfection according to the designer's requirements	Toe flash on the weld area	Toe flash on the weld area	Toe flash on the weld area
4	Linear misalignment	h ≤ 0,4 mm max 2 mm	0 mm	0 mm	0 mm
5	Underfill	h ≤ 0,2 mm max 0.5 mm	0.2 mm	0.5 mm	0.3 mm
6	Irregular width	Acceptable size of imperfection according to the designer's requirements	-	-	-
7	Irregular surface	Acceptable size of imperfection according to the designer's requirements	-	-	-

3.2 Radiography Interpretation

Figure 7(a) shows a radiographic image of the lateral tilt angle variation 0^0; it can be seen that the weld density had a relatively similar level of blackness (gray value). This suggests that the density level of the welding results on this material is the same [30]. Figure 7(b) illustrates an X-ray depicting a shift in lateral tilt angle of 0.5^0. The degree of blackness (gray value) of the weld's density was observable along a black line. The darkness intensity is greater at the center of the weld and diminishes towards the right. This suggests that the darker weld picture possesses a lower density than its surroundings, as a significant amount of radiation escapes and darkens the film in the weld material, which has a reduced density. Evidence suggests the presence of internal flaws characterized by cavities or tunneling measuring 10.5 cm in length. [9, 30-31]. The cause was the FSW tool rotating with a lateral tilt angle of 0.5^0, which rubbed the retreating side (RS) area, resulting in excessive heat. Still, the heat on the advancing side (AS) was reduced, so when the FSW tool began moving, little material was carried due to the lack of heat on the AS side. This is in accordance with the research of Mallieswaran et al [32]; the cause of tunneling is low plastic material displacement.

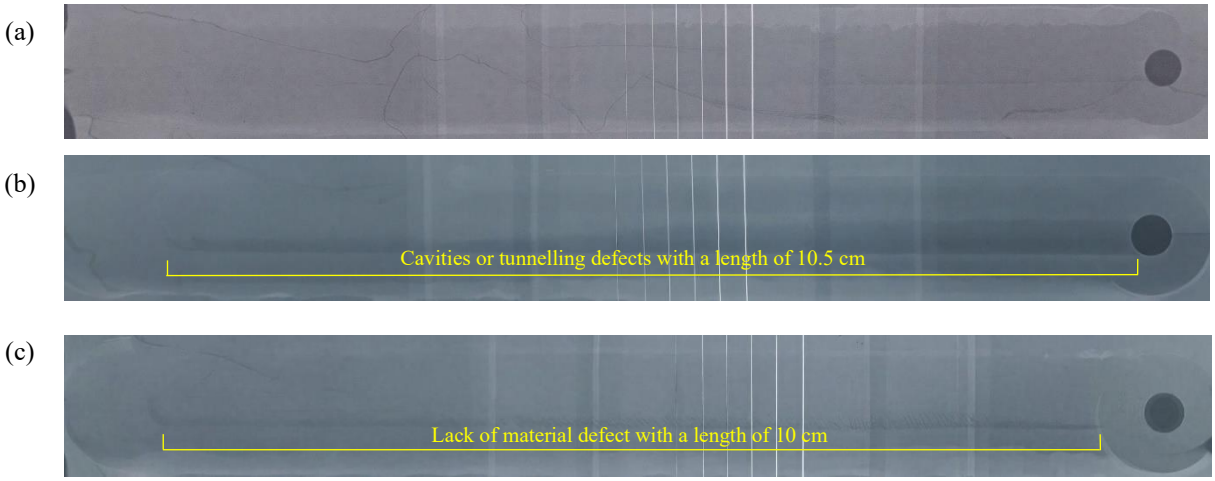

Figure 7. Interpretation of radiographic lateral tilt angles: (a) 0^0, (b) 0.5^0, (c) 1^0

In Figure 7(c), which shows the radiographic image of lateral tilt angle variation 1^0, it can be seen that the weld density has a relatively similar level of blackness (grey value). However, right in the middle of the weld, a blacker line is marked with a yellow line along the weld. This indicates that the actual weld image has a fairly even density, but the blacker straight line may indicate a section of the weld that is poorly integrated, particularly at the junction intended for connection with this friction weld; there is an indication of a lack of material with a length of 10 cm [9], the cause of lack of material is due to the lateral tilt angle of 1^0 causing excessive heat on the retreating side (RS), but causing a lack of heat in the advancing side (AS) area, so that the material carried by the tool has not fully reached the optimum temperature, causing a groove on one side (AS), because on one side the temperature is reduced. This is consistent with the research of Gel'atko et al. [33]: a decrease in heat input leads to an internal defect known as a material deficiency. The FSW radiographic interpretation at a lateral tilt angle of 0° shows that the weld had a consistent density, so these results were accepted. However, at lateral tilt angles of 0.5° and 1°, the density varied, suggesting the material is not uniform; therefore, another test, Eddy Current Testing (ECT), is required.

3.3 Edy Current Test Interpretation

Eddy current testing was carried out at three lateral tilt angles: 0^0, 0.5^0, and 1^0. Figure 8 displays the results of the eddy current test, which preceded quiet the radiographic test. Figure 8(a) displays the outcomes of eddy current testing with a lateral tilt angle change of 0^0. When the probe was pointed along the weld, the signal was usually stable, with no signal spikes due to a break in the weld material. This implies that the material exhibits homogeneity and lacks discontinuity. The findings of eddy current testing with a lateral tilt angle variation of 0.5^0 are displayed in Figure 8(b). No signal spikes were observed at breaks in the weld material, but the signal points moved to darker image densities, indicating tunneling or cavitation [33]. Figure 8(c) shows the results of eddy current testing with a lateral tilt angle variation of 1^0. There was no signal spike caused by discontinuity in the weld material, but there was a slight shift in the black line. Since no discontinuity (a kind of crack) in the weld can result in a signal spike, this deviation was not a substantial spike. The change in the signal point's position reflected a change in the material's density or unevenness. The eddy current test showed that at a lateral tilt angle of 0, the material was homogeneous with no discontinuities; at 0.50, the FSW results indicated tunneling or cavitation; and at $1^{0,\text{ the results}}$ indicated changes in density or unevenness in the material.

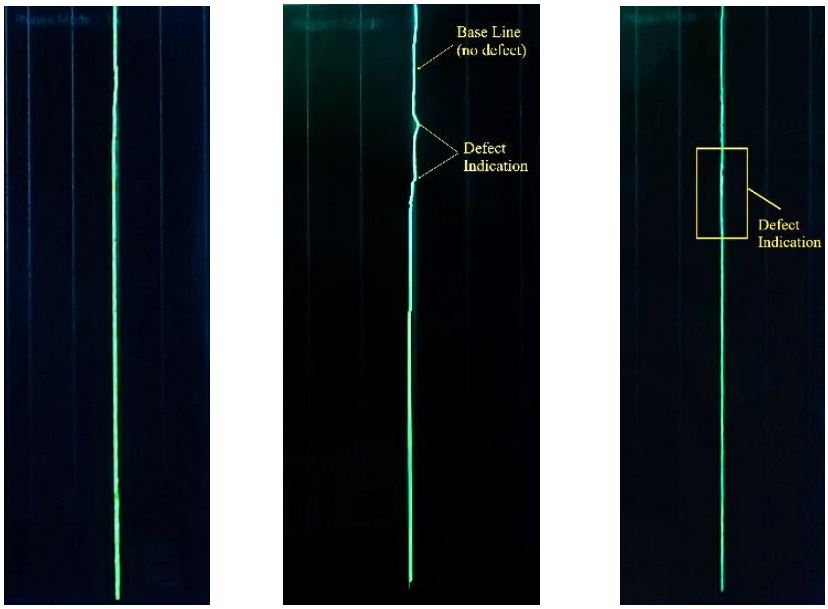

(a) lateral tilt angle 0^0 (b) lateral tilt angle $0.5^{0.}$ (c) lateral tilt angle 1^0

Figure 8. Interpretation of ECT lateral tilt angles at 500 kHz and 35 dB. The panels demonstrate tilt angles of (a) $0^{0,}$ (b) 0.5^0, and (c) 1^0

3.4 Tensile Strength

Details of the tensile test data are shown in Table 4. Figure 9 shows the specimens' UTS and joint efficiency graphs with the following tilt angles: 0.5^0 and 1^0. The highest tensile strength was obtained at a lateral tilt angle of 0^0, namely 85.53 MPa, with a joint efficiency of 78%. This is because the NDT results, presented as a visual test, indicated acceptance, and the radiography test confirmed that the material had a relatively uniform density and no defects. The eddy-current test revealed homogeneity and no discontinuities in the material. This is in accordance with Yang et al. [34]: uniform material flow results in a weld free of defects, thereby achieving optimal tensile strength. The lateral tilt angle variation of 0.5^0 results in a decrease in tensile strength to 61.84 MPa and a joint efficiency of 61.84%. This was evident from the NDT results, which showed an underfill of 0.5 mm, still within the criteria, as seen in the welding results in Figure 6(b). In particular, the bottom weld area showed the effect of underfill and uneven surface. Based on the radiography results, there

was an area in the middle of the weld that tended to be blacker; the farther to the right, the more extensive the blackness, indicating tunneling or a void. This was also demonstrated in the results of the eddy current testing, specifically in the blacker image density, where there was a shift in the position of the signal point that indicated tunneling or cavitation. This is consistent with the research by Yang et al. [34]; instability in the material flow can lead to tunneling defects, thereby reducing weld quality. Lateral tilt angle variation 1^0 had a higher tensile strength than the tilt angle variation of 0.5^0; this is due to insufficient material flow [34], with a value of 61.84 MPa and joint efficiency of 65.85%, but it was lower than the tilt angle variation of 0^0; this happened because the radiography test results showed less material. In addition, eddy current testing indicated changes in density or unevenness in the material. In the schematic of Figure 1, at lateral tilt angles of 0.5^0 and 1^0, the tool angle was directed to the retreating side (RS) so that excess heat was on that side. In contrast, on the advancing side (AS) there was a decrease in heat, when compared to the lateral tilt angle 0^0 where the tool side pressed the AS or RS which caused the heat produced evenly, so that the tilt angle 0.5^0 and 1^0 caused instability of the material flow when the tool started to move, in addition according to Mallieswaran et al [35], the stirr zone (SZ) area experienced grain refinement due to intense plastic deformation and recrystallization during the FSW process. In contrast, in the AS-TMAZ and RS-TMAZ areas, it produced imperfect recrystallization, resulting in lower mechanical properties than in the stirr zone (SZ). This was influenced by heat input through tool rotational speed, shoulder diameter, and tilt angle. This showed a decrease in tensile strength due to uneven heat from the tool, with lateral tilt angles of 0.5^0 and 1^0, which led to defect formation and reduced tensile strength. The lateral tilt angle variation indicated a decrease in tensile strength from 0^0 to 0.5^0 and an increase in tensile strength from 0.5^0 to 1^0, but when compared to 0^0, there was a decrease in tensile strength; this follows Yogaraj et al. [23] Increased heat in the tool and material, along with the increase in the tilt angle, causing plastic deformation and the occurrence of an imperfection flash, which caused its strength to decrease,. The material thickness decreases due to the flash [15, 28-29].

Table 4. Ultimate tensile strength and joint efficiency specimens

No.	Specimen	Specimen Code	Ultimate Tensile Strength (MPa)	Average Ultimate Tensile Strength (MPa)	Joint Efficiency (%)
1.	Raw Material	RM1	101.49	109.66	-
		RM2	117.81		
2.	Tilt angle 0^0	D1	77.98	85.53	78.00
		D2	93.09		
3.	Tilt angle 0.5^0	C1	56.24	67.81	61.84
		C2	79.37		
4.	Tilt angle 1^0	B1	64.91	71.91	65.58
		B2	78.91		

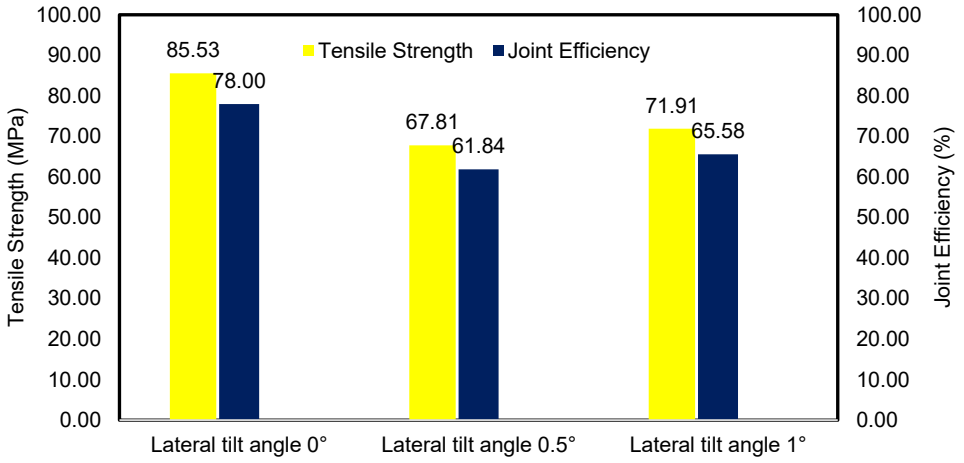

Figure 9. UTS and joint efficiency specimen

Figure 10 displays the tensile test fracture; Figure 10(a) displays the fracture with the highest tensile strength. This is evident from the straight fracture of the specimen, which shows uniform joint density and material homogeneity [30], leading to a uniform fracture. In the fracture area, necking was a ductile fracture pattern caused by the pin tool and the 0^0 tilt angle, producing moderate heat input, so it is free from defects [34], while Figure 10(b) shows the tensile test fracture with the lowest tensile strength. This can be seen from the multi-layered fracture, where the fracture process was not uniform but layer by layer. The tunnel defect that caused the fracture concentrated the stress flow in this defect section. Therefore, the initial crack starts from this defect [34]. According to Salih et al. [36], material density inhomogeneity is caused by the inability to mix metal during the welding phase. As shown by Choudhary et al. [30], the initial crack weakens the FSW joint and reduces its tensile strength, while Figure 10(c) illustrates a specimen fracture with medium

strength. This is evident from the multi-layered fracture shape in Figure 10(b), which shows a smaller defect intensity than in the specimen with a lateral tilt angle variation of 0.5^0. Mazzeschi et al. [31] also stated that this defect's presence causes nucleation and the spread of failure. Sabry et al. [37] noted that the initial point of cracking due to voids is inadequate material flow, resulting in weak bonds. These fracture findings support earlier NDT tests, which showed that specimens with a lateral tilt angle variation of 0^0 had perfect weld quality, those with a lateral tilt angle variation of 0.5^0 had the most serious weld defects, and specimens with a lateral tilt angle variation of 1^0 had relatively minor defects with a lateral tilt angle variation of 0.5^0

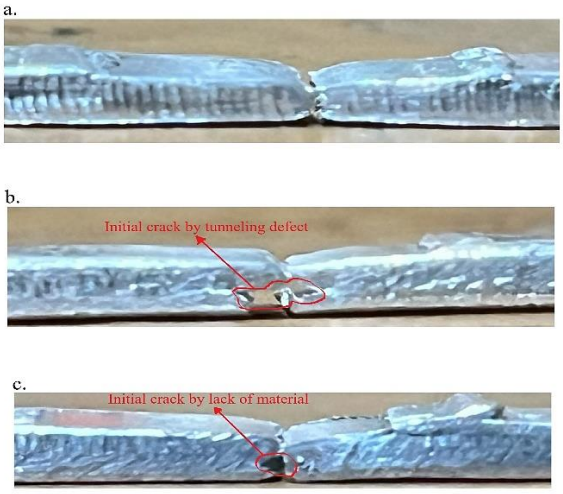

Figure 10. Tensile test fracture samples: (a) lateral tilt angle of 0^0, (b) lateral tilt angle of 0.5^0, and (c) lateral tilt angle of 1^0

4. Conclusions

The results demonstrate the quality of FSW on thin plate aluminum 1100 with lateral tilt angles of 0^0, 0.5^0, and 1^0; at 0^0, no defects were observed, whereas at 0.5^0 and 1^0, defects were present. The highest tensile strength at a lateral tilt angle variation of 0^0 is 85.53 MPa, with a joint efficiency of 78%. Due to the homogeneous material and the absence of discontinuities, there was a decrease in tensile strength at a lateral tilt angle of 0.5^0, to 61.84 MPa, with a joint efficiency of 61.84%. This reduction was due to indications of tunneling or voids. There was an increase in tensile strength at a lateral tilt angle of 1^0 compared to the tensile strength at a lateral tilt angle of 0.5^0, with (91 MPa with a joint efficiency of 65.85%, b), but there was a decrease when compared to the tensile strength at a lateral tilt angle 0^0. This was due to changes in density or unevenness in the material. Tensile test fractures at the three side lateral tilt angles confirmed the nondestructive test results, indicating no defects in the 0^0 variation but defects in the 0.5^0 and 1^0 variations. The FSW process is applied in this research to aircraft oil tanks, so outstanding welding quality is required to produce this product. According to ISO 25239-4, the joint efficiency for pure aluminum must reach 100%. Therefore, further research is needed, especially on tool design to avoid underfilling, which can reduce tensile strength, as well as on tool design to produce defect-free welds.

Acknowledgements

The researcher would like to thank the Department of Mechanical Engineering at Semarang State University for its support in this research on the friction stir welding process.

Funding

This study was not supported by any grants from funding bodies in the public, private, or not-for-profit sectors.

Declaration of Competing Interest

The author declares no conflicts of interest.

CRediT Authorship Contribution Statement

Febri Budi Darsono (Conceptualization; Methodology; Formal analysis; Writing - original draft)
Akhmad Nurdin (Data curation)
Fajar Paundra (Data curation)
Alvreando Kaleb Thomas (Data curation)
Tasih Mulyono (Formal analysis; Visualization; Investigation)
Muhammad Irfan Nuryanta (Resources)
Hendrix Noviyanto Firmnsyah (Data curation; Resources)
Aldias Bahatmaka (Data curation; Resources; Supervision)

Deni Fajar Fitriyana (Writing - review & editing)
Kriswanto (Writing - review & editing)
Rahmat Doni Widodo (Writing - review & editing)
Nurul Muhayat (Writing - review & editing)

Availability of Data and Materials
The data supporting this study's findings are available on request from the corresponding author.

Ethics Declarations
This study did not involve human participants or animals. Ethical approval was therefore not required.

Generative Artificial Intelligence Declarations
The authors claim that artificially intelligent-assisted technologies, such as generative AI, were not used to generate content, ideas, or theories. We have just utilized AI to enhance readability and refine the language. This was used with extreme human control and oversight. The authors take full responsibility for reviewing and approving the content.

References

[1] G. Tiwari, N. Khaire, M.A. Iqbal, P.K. Gupta, N.K. Gupta, "Ballistic response of double-layered 1100-H12 aluminium hemispherical shell structure," *Thin-Walled Structures*, vol. 148, p. 106619, 2020.
[2] E. H. Parker-Quaife, C. Verst, C. R. Heathman, P. R. Zalupski, and G. P. Horne, "Radiation-induced molecular hydrogen gas generation in the presence of aluminum alloy 1100," *Radiation Physics and Chemistry*, vol. 177, p. 109117, 2020.
[3] C.H. Ng, S.N.M. Yahaya, A.A.A. Majid, "Reviews on aluminum alloy series and its applications," *Academia Journal of Scientific Research*, vol. 5, no. 12, pp. 708–716, 2017.
[4] M. Khan, R. Ud-Din, A. Wadood, W.H. Syed, S. Akhtar, R.E. Aune, "Spark plasma sintering of graphene nanoplatelets reinforced aluminium 6061 alloy composites," in *Light Metals 2020*, pp. 301–311, 2020.
[5] M. Khan, R. ud Din, M. Abdul Basit, A. Wadood, S. Wilayat Husain, S. Akhtar, et al., "Effects of graphene nanoplatelets and boron carbide on microstructure and mechanical behaviour of aluminium alloy (Al6061) after friction stir welding," *Advances in Materials and Processing Technologies*, vol. 8, no. 3, pp. 3148–3164, 2022.
[6] G. Ipekoğlu, G. Çam, "Formation of weld defects in cold metal transfer arc welded 7075-T6 plates and its effect on joint performance," in *IOP Conference Series: Materials Science and Engineering*, Institute of Physics Publishing, Oct. 2019.
[7] G. Çam,M. Koçak, "Microstructural and mechanical characterization of electron beam welded Al-alloy 7020," *J Mater Sci*, vol. 42, pp. 7154–7161, 2007.
[8] G. Çam, V. Ventzke, J.F. Dos Santos, M. Koçak, G. Jennequin, P. Gonthier-Maurin, "Characterisation of electron beam welded aluminium alloys," *Science and Technology of Welding and Joining*, vol. 4, no. 5, pp. 317–323, 1999.
[9] M.U.F. Awan, M. Khan, K. Waheed, Z. Iqbal, A. Rehman, F. Ali, et al., "Parametric optimisation of friction stir welding on aluminium alloy (EN AW-1100) plates," *Acta Polytechnica*, vol. 63, no. 2, pp. 75–88, 2023.
[10] C.J. Dawes, "Friction stir process welds aluminum alloys," *Weld J*, vol. 36, 1995.
[11] R.S. Mishra, Z.Y. Ma, "Friction stir welding and processing," *Materials science and engineering: R: reports*, vol. 50, no. 1–2, pp. 1–78, 2005.
[12] K. Elangovan, V. Balasubramanian, "Influences of tool pin profile and tool shoulder diameter on the formation of friction stir processing zone in AA6061 aluminium alloy," *Mater Des*, vol. 29, no. 2, pp. 362–373, 2008.
[13] S. Verma, V. Kumar, R. Kumar, R.S. Sidhu, "Exploring the application domain of friction stir welding in aluminum and other alloys," *Mater Today Proc*, vol. 50, pp. 1032–1042, 2022.
[14] A.C.F. Silva, D.F.O. Braga, M.A. V De Figueiredo, P. Moreira, "Ultimate tensile strength optimization of different FSW aluminium alloy joints," *The International Journal of Advanced Manufacturing Technology*, vol. 79, pp. 805–814, 2015.
[15] F. Budi Darsono, S. T. Koin, K. Kriswanto, A. K. Thomas, R. D. Widodo, and R. Rusiyanto, "Effect of Pin Profile Tool on Friction Stir Welding Alumunium," in *E3S Web of Conferences*, 2023.
[16] N. Muhayat, M.S. Harjono, Y.P.D.S. Depari, A.R. Prabowo, T. Triyono, E.D.W.S. Putri, et al., "Friction stir welded AA5052-H32 under dissimilar pin profile and preheat temperature: microstructural observations and mechanical properties," *Metals (Basel)*, vol. 12, no. 1, p. 4, 2021.
[17] R.M. Vaidyanathan, N. Sivaraman, M. Patel, M.M. Woldegioris, T.A. Atiso, "A review on the effects of shoulder diameter to pin diameter (D/d) ratio on friction stir welded aluminium alloys," *Mater Today Proc*, vol. 45, pp. 4792–4798, 2021.
[18] M. Mehta, A. Arora, A. De, T. DebRoy, "Tool geometry for friction stir welding—optimum shoulder diameter," *Metallurgical and Materials Transactions A*, vol. 42, pp. 2716–2722, 2011.
[19] R. Kumar, H. Kumar, S. Kumar, J.S. Chohan, "Effects of tool pin profile on the formation of friction stir processing zone in AA1100 aluminium alloy," *Mater Today Proc*, vol. 48, pp. 1594–1603, 2022.
[20] S. Ahmed, P. Saha, "Development and testing of fixtures for friction stir welding of thin aluminium sheets," *J Mater Process Technol*, vol. 252, pp. 242–248, 2018.

[21] A. Tsarkov, K. Trukhanov, I. Zybin, A. Vichniakov, "Tilt Angle Effect on Friction Stir Welding Conditions," *Key Eng Mater*, vol. 910, pp. 115–122, 2022.
[22] N. Dialami, M. Cervera, M. Chiumenti, "Effect of the tool tilt angle on the heat generation and the material flow in friction stir welding," *Metals (Basel)*, vol. 9, no. 1, p. 28, 2018.
[23] P. Yogaraj L. Kasirajan, "Identifying the Optimal Process Parameter on AA1100 Friction Stir Welded Joints," *Tehnički vjesnik*, vol. 29, no. 3, pp. 957–964, 2022.
[24] I. Radisavljevic, A. Zivkovic, N. Radovic, V. Grabulov, "Influence of FSW parameters on formation quality and mechanical properties of Al 2024-T351 butt welded joints," *Transactions of Nonferrous Metals Society of China*, vol. 23, no. 12, pp. 3525–3539, 2013.
[25] C. Wu, J. Wang, Q. Wang, P. Xia, D. Li, "7075 aluminum alloy Friction Stir Welding (FSW): Quality analysis and mechanical properties with WC-Co tool," *Mater Today Commun*, vol. 38, p. 108203, 2024.
[26] ISO, "PN-EN ISO 25239-5," *Friction stir welding. Aluminium. Part 5: Quality and inspection requirements*, 2012.
[27] ASTM, "ASTM E8 -Test Methods for Tension Testing of Metallic Materials," May 01, 2022, *ASTM International, West Conshohocken, PA*.
[28] A. Tamadon, A. Baghestani, M.E. Bajgholi, "Influence of WC-based pin tool profile on microstructure and mechanical properties of AA1100 FSW welds," *Technologies (Basel)*, vol. 8, no. 2, p. 34, 2020.
[29] N.M. Abdeltawab, M. Elshazly, A.Y. Shash, M. El-Sherbiny, "Studying the effect of processing parameters on the microstructure, strength, hardness, and corrosion characteristics of friction stir dissimilar welded AA5083 and AA7075 aluminum alloys reinforced with Al-SiC matrix," *Heliyon*, vol. 11, no. 1, p. e41362, 2025.
[30] A.K. Choudhary R. Jain, "Influence of stir zone temperature and axial force on defect formation and their effect on weld efficiency during friction stir welding of AA1100: A simulation and experimental investigation," *Mater Today Commun*, vol. 37, p. 107413, 2023.
[31] M. Mazzeschi, M. Sanz, J.C. Monge, E. Cañibano, C.P. Rodriguez-Juan, K.C. Núñez, "Electrical conductivity field analysis: A prognostic instrument for real-time monitoring of friction stir welding process," *J Manuf Process*, vol. 131, pp. 93–110, 2024.
[32] K. Mallieswaran, R. Padmanabhan, V. Balasubramanian, "Friction stir welding parameters optimization for tailored welded blank sheets of AA1100 with AA6061 dissimilar alloy using response surface methodology," *Advances in Materials and Processing Technologies*, vol. 4, no. 1, pp. 142–157, 2018.
[33] M. Geľatko, M. Hatala, F. Botko, R. Vandžura, J. Hajnyš, "Study of Eddy Current Testing Ability on SLM Aluminium Alloy," *Materials*, vol. 17, no. 14, 2024.
[34] S. Yang, S. Chen, H. Song, J. Shen, "Effects of tool geometry on the weld quality of friction stir welded ultra-thin 1060 aluminum alloy plate," *International Journal of Lightweight Materials and Manufacture*, 2025.
[35] K. Mallieswaran, S. Agaramudhalvan, D.G. Oliver, "Microstructural stability and strength correlation in AGG-affected friction stir welded AA2024-T4 joints," *Advances in Materials and Processing Technologies*, vol. 0, pp. 1–10, 2025.
[36] O. S. Salih, H. Ou, W. Sun, "Heat generation, plastic deformation and residual stresses in friction stir welding of aluminium alloy," *Int J Mech Sci*, vol. 238, p. 107827, 2023.
[37] I. Sabry, "Exploring the effect of friction stir welding parameters on the strength of AA2024 and A356-T6 aluminum alloys," *Journal of Alloys and Metallurgical Systems*, vol. 8, p. 100124, 2024.